運輸省港湾技術研究所

港湾技術研究所
報告

REPORT OF
THE PORT AND HARBOUR RESEARCH
INSTITUTE

MINISTRY OF TRANSPORT
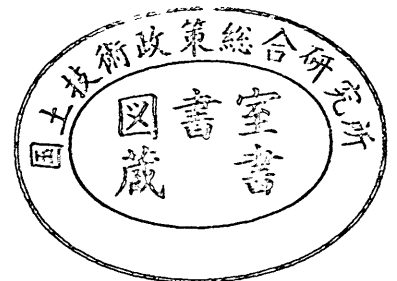
NAGASE, YOKOSUKA, JAPAN

港湾技術研究所報告 (REPORT OF P.H.R.I.)

目　次 (CONTENTS)

Nonlinear Model for Wave Fields with Current

Md. Hasanat ZAMAN *

Tetsuya HIRAISHI *

Synopsis

A two-dimensional numerical model has been formulated to study nonlinear wave-current coexistence field. The governing equations of the model are obtained through the vertical integration of the continuity equation and the equations of motions. A semi-implicit finite difference scheme is proposed for the numerical solution of the resulted equations. As an application, the model is employed to a vertically two-dimensional wave-current field with a bottom obstacle of parabolic cross section. Flow separation phenomenon is treated geometrically in the frame of non-breaking wave motion. The comparisons of the numerical results show great agreement with the experimental data.

Keywords : Nonlinear models, Wave-current coexistence, Bottom obstacle, Physical
          experiments

* Wave laboratory, Hydraulic Engineering Division
  (3-1-1Nagase, Yokosuka, Kanagawa, Japan239-0826
  Tel : +81-468-44-5063, Fax : +81-468-41-3888, Email : zaman@cc.phri.go.jp

流れが考慮できる非線形波浪の計算モデルについて

エムディ. ハサナット　ジャーマン・平石哲也 *

要　旨

　非線形な波・流れ共存場に適用できる二次元数値計算モデルを構築した．モデルの支配方程式は鉛直方向に積分した連続式と運動方程式である．支配方程式を半陰的有限差分法により差分化した．底面に設置した放物型マウンド周辺の鉛直二次元波・流れ場にこのモデルを適用し，非砕波条件下におけるマウンド周りの剥離流れの特性を空間的に検討した．数値計算モデルによる結果は模型実験による結果と非常によく一致した．

キーワード：非線形モデル，波・流れの共存場，マウンド，模型実験

---

* 水工部波浪研究室

　(〒239-0826　神奈川県横須賀市長瀬3-1-1，Tel：0468-44-5063，Fax：0468-41-3888，
　E-mail：zaman@cc.phri.go.jp zaman@cc.phri.go.j)

CONTENTS

1. Introduction

A great amount of open land all over the world is the nearshore zone including the beach. The increasing population of the world has already started to capture the nearshore area for accommodation, business and other recreational purposes. Thus, researches for reliable prediction of nearshore dynamic process and their resulting beach topographic change have been boosted both numerically and experimentally during the last decades. The land-use practice around the coastal territory is still under of low priority in terms of caution as it involves considerable risk to the lives, properties and marine environment. A better understanding of the localized flow conditions and their resulting impact over the nearshore zone is obviously necessary in order to achieve sufficient knowledge to protect the territory, local inhabitants and environment. In reality water motion can exist only in the form of wave and current and most of the nearshore dynamic processes such as sediment transport and the resulting beach topographic change, etc. are directly influenced by the wave, current and their combined effects. Thus wave-current coexistence field has grown as one of the most important topic in the Coastal Engineering subject during the last decades and, therefore, of great interest for the coastal engineers to design coastal structures and to predict their functional performance. Engineers and researchers have been advancing their researches to understand the exact phenomenon as close as possible. During the last decades, a lot of outstanding contributions, both theoretically and experimentally were made to this field by different investigators. Many of these theories have received substantial acceptance for the evaluation of the wave-current field under particular waves, currents and bathymetry conditions.

As mentioned by Hedges (1987) that traditionally, it is the practice of the engineers to neglect the presence of current in the wave field and as an assumption, the interaction between the wave and current is almost always avoided. This type of assumption may be authentic where the velocity of the current is minimal but might be dangerous when the current is stronger than to be neglected. This is because, the presence of current alters the wave characteristics significantly upon the bottom contour, leads to noticeable errors in the computation of the integrated flow pattern. Hedges also stressed that the interaction among waves and currents must be carefully considered when it comes to calculate wave height from the subsurface pressure recordings, refraction and defraction calculation, forces on the ocean structure and energy spectra. Horikawa (1988) acknowledged that the existing mathematical models are hardly being assessed due to insufficient experimental or prototype data. After long time of Horikawa, Ribberink et al. (1994) lamented reporting that adequate knowledge on the interaction between waves, currents, sediments and the seabed in the combined wave-current field does not exist yet. Longuet-Higgins and Stewart (1961, 1962, 1963 and 1964) derived theoretical expressions for the changes in sea level and other linear and nonlinear characteristics of the wave trains considering the radiation stress mechanism. The radiation stress concept proposed by Longuet-Higgins and Stewart needs successive iteration for the computation of the wave-induced current that demands high computational efforts along with high possibility of numerical errors.

Brevik and Aas (1980) termed the 'Radiation stress' concept as a confusing one and developed their wave-current model following the energy conservation law. In the same paper they experimentally showed the reduction of the mean horizontal velocity profile in the wave-current system as compared to the case of undisturbed current. Ismail (1983) stressed that for the case of a following current, the use of depth average current for an irrotational wave-current model is reasonable, as the waves tend to decrease the vertical velocity gradient of the shear flow. On the other hand, for the reverse current, he adds, as the waves tend to increase the vertical shear of current velocity profile, so a linear shear current model should be used for the sufficiently accurate solution. Hedges and Lee (1991) showed that a depth varying current can be replaced by an 'equivalent uniform current' under the conditions of approximate constant current vorticity and the 'equivalence constant (ε)' must be smaller than the relative water depth. The use of Boussinesq equation has received considerable attention for the computation of wave [McCowan (1987), Madsen et al. (1992), and, Schäffer and Madsen (1995)] and wave-current system [Yoon and Liu (1989), Sato

and Kabiling (1994), Sφrensen *et al.* (1994) and Watanabe *et al.* (1994)], but still these types of models are not yet widely applicable for the considerably deep water. Boussinesq equation based model also needs dense grid points for better prediction that affects the computational time. Thus a more generally applicable numerical method is necessary to directly discern the combined effects of waves, currents and their resultant effects.

In this study, a horizontally two-dimensional semi-implicit mathematical model is developed and presented. Later the model is transformed to a one-dimensional form and applied to a vertically two-dimensional wave-current coexistence field. The comparisons of the model results with experimental data are presented and discussed

2. Governing Equations

During formulation of the governing equations inviscid and incompressible fluid motion has been assumed. Consequently, the following continuity equation and the equations of motions can describe the wave motion:

$$\frac{\partial u}{\partial x} + \frac{\partial v}{\partial y} + \frac{\partial w}{\partial z} = 0 \tag{1}$$

$$\frac{\partial u}{\partial t} + u\frac{\partial u}{\partial x} + v\frac{\partial u}{\partial y} + w\frac{\partial u}{\partial z} + \frac{1}{\rho}\frac{\partial p_d}{\partial x} + \varepsilon(x)u = 0 \tag{2}$$

$$\frac{\partial v}{\partial t} + u\frac{\partial v}{\partial x} + v\frac{\partial v}{\partial y} + w\frac{\partial v}{\partial z} + \frac{1}{\rho}\frac{\partial p_d}{\partial y} + \varepsilon(y)v = 0 \tag{3}$$

where u, v and w are the velocity components in the x, y and z directions, respectively; ρ is the water density, t the time and p_d is the dynamic pressure.

The terms $\varepsilon(x)$ and $\varepsilon(y)$ in the equations of motions are the boundary damping function which is uniform along the y direction and linearly varies along the x direction. This damping function can be formulated as follows:

$$\varepsilon(x) = \frac{R\varepsilon_m}{2(\sinh R - R)}\left[\cosh(Rx/G) - 1\right] \tag{4}$$

where damping coefficient, $\varepsilon_m = \sqrt{gh}$, $R = 3$ is a coefficient, G is usually taken 2~3 wavelengths and g is the gravitational acceleration. Apart from the boundary the damping coefficient is null elsewhere.

The velocity potential (*see* also Dean and Dalrymple 1992) for the case when a time periodic wave motion is superimposed over a two dimensional wave-current field can be expressed as follows:

$$\phi = U_j x_j + A\cosh k(h + z)\cos(k_j x_j - \sigma t) + C(t) \tag{5}$$

where U_j ($j = x,y$) are the current velocity in the x and y direction, h the still water depth; k is the resultant wave number-resemble parameter in which k_j ($j = x,y$) are its components in the x and y directions, σ the angular frequency, t the time, g the acceleration due to gravity. x_j ($j = x,y$) are the horizontal and z is the vertical coordinate and, A is a

constant related to the wave height. The modification to the wave number is necessary to include the instantaneous water depth instead of mean water depth in order to consider moderately large wave amplitudes.

Now the surface elevation η can be formulated from the dynamic free surface boundary condition in the following way:

$$\eta = -\frac{1}{g}\left[\frac{\partial\phi}{\partial t} + \frac{1}{2}\left(\frac{\partial\phi}{\partial x}\right)^2 + \frac{1}{2}\left(\frac{\partial\phi}{\partial y}\right)^2 + \frac{1}{2}\left(\frac{\partial\phi}{\partial z}\right)^2\right]_{z=\eta} \tag{6}$$

When Eq.5 is invoked and all the terms associated with $A^2 k_x^2$ and $A^2 k_y^2$ are neglected due to smaller values of wave induced horizontal velocity components, the final form of η is evaluated as:

$$\eta = -\frac{A\sigma}{g}\left[1 - \frac{U_j k_j}{\sigma}\right]\cosh k(h+\eta)\sin(k_j x_j - \sigma t) \tag{7}$$

In the similar fashion the dispersion relation for a combined wave-current coexistence field can be explored from the kinematic boundary condition:

$$\frac{\partial\eta}{\partial t} + \frac{\partial\phi}{\partial x}\frac{\partial\eta}{\partial x} + \frac{\partial\phi}{\partial y}\frac{\partial\eta}{\partial y} - \frac{\partial\phi}{\partial z} = 0 \tag{8}$$

After using Eqs.5 and 6 in Eq.8, the dispersion relation evolves into the following form:

$$\frac{\sigma^2}{gk}\left(1 - \frac{k_j U_j}{\sigma}\right)^2 = \tanh k(h+\eta) \tag{9}$$

When the expressions for ϕ and η are known, the equation for dynamic pressure can be obtained from the Bernoulli equation:

$$\frac{p_d}{\rho} = -\left[\frac{\partial\phi}{\partial t} + \frac{1}{2}\left(\frac{\partial\phi}{\partial x}\right)^2 + \frac{1}{2}\left(\frac{\partial\phi}{\partial y}\right)^2 + \frac{1}{2}\left(\frac{\partial\phi}{\partial z}\right)^2\right] \tag{10}$$

Invoking Eqs.5 and 7, the expression for dynamic pressure takes the following shape:

$$p_d = \rho g\eta\frac{\cosh k(h+z)}{\cosh k(h+\eta)} \tag{11}$$

The kinematic free surface and bottom boundary conditions are expressed by the following equations where superscript s or b, respectively, stands for the quantity at the free surface or at the bottom:

$$\frac{\partial \eta}{\partial t} + u_j^s \frac{\partial \eta}{\partial x_j} - w^s = 0 \tag{12}$$

$$u_j^b \frac{\partial h}{\partial x_j} + w^b = 0 \tag{13}$$

Now the vertical integration of the continuity equation (Eq.1) and the equation of motions (Eqs.2 and 3) are carried out along with invoking Eqs.12 and 13 to give the following governing equations.

From the continuity equation:

$$\eta_t + P_x + Q_y = 0 \tag{14}$$

From the x and y direction momentum equation:

$$P_t + \left[\frac{P^2 \chi}{h+\eta}\right]_x + \left[\frac{PQ\chi}{h+\eta}\right]_y + \left[\eta g \alpha_1^x + C\right]\eta_x + \left[\eta g \alpha_2^x\right]h_x + \varepsilon(x)P = 0 \tag{15}$$

$$Q_t + \left[\frac{PQ\chi}{h+\eta}\right]_x + \left[\frac{Q^2 \chi}{h+\eta}\right]_y + \left[\eta g \alpha_1^y + C\right]\eta_y + \left[\eta g \alpha_2^y\right]h_y + \varepsilon(y)Q = 0 \tag{16}$$

where the subscripts x, y and t stand for partial differentiation operator. $P = \int_{-h}^{\eta} u \, dz$ and $Q = \int_{-h}^{\eta} v \, dz$ are the flux per unit width in the x and y direction, respectively; χ is the momentum correction factor and C is the wave celerity; α_1^x, α_2^x and α_1^y, α_2^y are the relative water depth dependent parameter in the x and y direction, respectively and can be expressed as:

$$\chi = \frac{1}{2}\left[\frac{k(h+\eta)}{\tanh k(h+\eta)}\right]\left[1 + \frac{2k(h+\eta)}{\sinh 2k(h+\eta)}\right] \tag{17}$$

$$\alpha_1^x = X - 1 \tag{18}$$

$$\alpha_2^x = X - \frac{1}{\cosh k(h+\eta)} \tag{19}$$

$$\alpha_1^y = Y - 1 \tag{20}$$

$$\alpha_2^y = Y - \frac{1}{\cosh k(h+\eta)} \tag{21}$$

and,

$$X = \left[\frac{2 \tanh k(h+\eta) + \dfrac{2\sigma U_x}{g} \cos \theta_w \left(1 - \dfrac{k_j U_j}{\sigma}\right)}{k(h+\eta) + \dfrac{1}{2}\sinh 2k(h+\eta) + \dfrac{2\sigma U_x}{g} \cos \theta_w \left(1 - \dfrac{k_j U_j}{\sigma}\right) \cosh^2 k(h+\eta)} \right] \tag{22}$$

$$Y = \left[\frac{2 \tanh k(h+\eta) + \dfrac{2\sigma U_y}{g} \sin \theta_w \left(1 - \dfrac{k_j U_j}{\sigma}\right)}{k(h+\eta) + \dfrac{1}{2}\sinh 2k(h+\eta) + \dfrac{2\sigma U_y}{g} \sin \theta_w \left(1 - \dfrac{k_j U_j}{\sigma}\right) \cosh^2 k(h+\eta)} \right] \tag{23}$$

In the above equations θ_w is the wave inclination.

Finally, we obtained Eqs.14, 15 and 16 as our governing equations for the wave-current field.

2.1 Numerical scheme

The governing equations just obtained have been discretized following a semi-implicit technique (Zaman and Togashi, 1997). The discretization of the governing equations is carried out following the mesh shown in **Figure 1**. The nonlinear convective terms in the momentum equations are properly linearized and expressed by the defined values of the unknowns. The present scheme is very direct and efficient as Eq.24 does the computation of the surface elevation, which is explicit in nature. The momentum equation for each direction constitutes a tridiagonal coefficient matrix in every time step, which can be solved by the double sweep algorithm. .

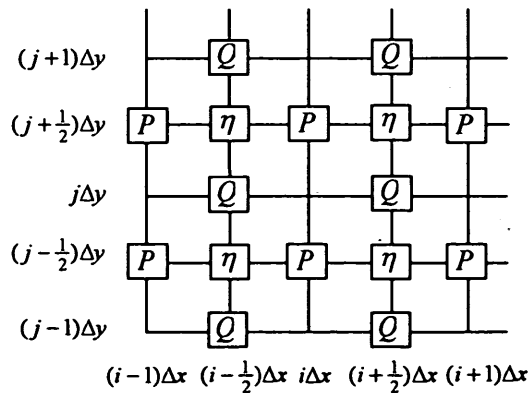After the discretization, Eq.14, 15 and 16, respectively, takes the following forms:

Figure 1 Definition sketch of the two-dimensional computational mesh

$$\eta^{n+1}_{i-\frac{1}{2},J+\frac{1}{2}} = \eta^{n}_{i-\frac{1}{2},J-\frac{1}{2}} - \frac{\Delta t}{\Delta s}\left[P^{n+\frac{1}{2}}_{i,J-\frac{1}{2}} - P^{n+\frac{1}{2}}_{i-1,J-\frac{1}{2}}\right] - \frac{\Delta t}{\Delta s}\left[Q^{n+\frac{1}{2}}_{i-\frac{1}{2},J} - Q^{n+\frac{1}{2}}_{i-\frac{1}{2},J-1}\right] \tag{24}$$

$$a^{n+1}_{xi,J-\frac{1}{2}}P^{n+\frac{3}{2}}_{i-1,J-\frac{1}{2}} + b^{n+1}_{xi,J-\frac{1}{2}}P^{n+\frac{3}{2}}_{i,J-\frac{1}{2}} + c^{n+1}_{xi,J-\frac{1}{2}}P^{n+\frac{3}{2}}_{i+1,J-\frac{1}{2}} = d^{n+1}_{xi,J-\frac{1}{2}} \tag{25}$$

$$a^{n+1}_{yi-\frac{1}{2},J}Q^{n+\frac{3}{2}}_{i-\frac{1}{2},J-1} + b^{n+1}_{yi-\frac{1}{2},J}Q^{n+\frac{3}{2}}_{i-\frac{1}{2},J} + c^{n+1}_{yi-\frac{1}{2},J}Q^{n+\frac{3}{2}}_{i-\frac{1}{2},J+1} = d^{n+1}_{yi-\frac{1}{2},J} \tag{26}$$

where the constants are defined as:

$$a^{n+1}_{xi,J-\frac{1}{2}} = -\frac{\Delta t}{4\Delta S}\left[\left(\frac{\chi}{h+\eta}\right)^{n+1}_{i-\frac{1}{2},J-\frac{1}{2}}\left(P^{n+\frac{1}{2}}_{i,J-\frac{1}{2}} + P^{n+\frac{1}{2}}_{i-1,J-\frac{1}{2}}\right)\right] \tag{27}$$

$$c^{n+1}_{xi,J-\frac{1}{2}} = \frac{\Delta t}{4\Delta S}\left[\left(\frac{\chi}{h+\eta}\right)^{n+1}_{i+\frac{1}{2},J-\frac{1}{2}}\left(P^{n+\frac{1}{2}}_{i+1,J-\frac{1}{2}} + P^{n+\frac{1}{2}}_{i,J-\frac{1}{2}}\right)\right] \tag{28}$$

$$b^{n+1}_{xi,J-\frac{1}{2}} = 1 + a^{n+1}_{xi,J-\frac{1}{2}} + c^{n+1}_{xi,J-\frac{1}{2}} + \frac{1}{2}\varepsilon_{i,J-\frac{1}{2}} \tag{29}$$

$$d^{n+1}_{xi,J-\frac{1}{2}} = P^{n+\frac{1}{2}}_{i,J-\frac{1}{2}} - \frac{\Delta t}{4\Delta S}\left[\left(\frac{\chi}{h+\eta}\right)^{n+1}_{i-\frac{1}{2},J+\frac{1}{2}}\left(P^{n+\frac{1}{2}}_{i,J+\frac{1}{2}} + P^{n+\frac{1}{2}}_{i-1,J+\frac{1}{2}}\right)\left(Q^{n+\frac{1}{2}}_{i-\frac{1}{2},J+1} + Q^{n+\frac{1}{2}}_{i-\frac{1}{2},J}\right)\right]$$

$$+ \frac{\Delta t}{4\Delta S}\left[\left(\frac{\chi}{h+\eta}\right)^{n+1}_{i-\frac{1}{2},J-\frac{1}{2}}\left(P^{n+\frac{1}{2}}_{i,J-\frac{1}{2}} + P^{n+\frac{1}{2}}_{i-1,J-\frac{1}{2}}\right)\left(Q^{n+\frac{1}{2}}_{i-\frac{1}{2},J} + Q^{n+\frac{1}{2}}_{i-\frac{1}{2},J-1}\right)\right]$$

$$- \frac{\Delta t}{2\Delta S}\left[\left(ng\alpha^{x}_{1} + C^{2}\right)^{n+1}_{i+\frac{1}{2},J-\frac{1}{2}} + \left(ng\alpha^{x}_{1} + C^{2}\right)^{n+1}_{i-\frac{1}{2},J-\frac{1}{2}}\right]$$

$$\cdot\left[\left\{\eta^{n+1}_{i+\frac{1}{2},J-\frac{1}{2}} - \eta^{n+1}_{i-\frac{1}{2},J-\frac{1}{2}}\right\}\right] - \frac{\Delta t}{2\Delta S}\left[\left(ng\alpha^{x}_{2}\right)^{n+1}_{i+\frac{1}{2},J-\frac{1}{2}} + \left(ng\alpha^{x}_{2}\right)^{n+1}_{i-\frac{1}{2},J-\frac{1}{2}}\right]$$

$$\cdot\left[\left\{h^{n+1}_{i+\frac{1}{2},J-\frac{1}{2}} - h^{n+1}_{i-\frac{1}{2},J-\frac{1}{2}}\right\}\right] - \frac{1}{2}\varepsilon_{i,J-\frac{1}{2}}P^{n}_{i,J-\frac{1}{2}} \tag{30}$$

$$a^{n+1}_{yi-\frac{1}{2},J} = -\frac{\Delta t}{4\Delta S}\left[\left(\frac{\chi}{h+\eta}\right)^{n+1}_{i-\frac{1}{2},J-\frac{1}{2}}\left(Q^{n+\frac{1}{2}}_{i-\frac{1}{2},J} + Q^{n+\frac{1}{2}}_{i-\frac{1}{2},J-1}\right)\right] \tag{31}$$

$$c^{n+1}_{yi-\frac{1}{2},J} = \frac{\Delta t}{4\Delta S}\left[\left(\frac{\chi}{h+\eta}\right)^{n+1}_{i-\frac{1}{2},J+\frac{1}{2}}\left(Q^{n+\frac{1}{2}}_{i-\frac{1}{2},J+1} + Q^{n+\frac{1}{2}}_{i-\frac{1}{2},J}\right)\right] \tag{32}$$

$$b^{n+1}_{i-\frac{1}{2},j} = 1 + a^{n+1}_{i-\frac{1}{2},j} + c^{n+1}_{i-\frac{1}{2},j} + \frac{1}{2}\varepsilon_{i-\frac{1}{2},j} \qquad (33)$$

$$d^{n+1}_{i-\frac{1}{2},j} = Q^{n+\frac{1}{2}}_{i-\frac{1}{2},j} - \frac{\Delta t}{4\Delta S}\left[\left(\frac{\chi}{h+\eta}\right)^{n+1}_{i+\frac{1}{2},j-\frac{1}{2}}\left(P^{n+\frac{1}{2}}_{i+1,j-\frac{1}{2}} + P^{n+\frac{1}{2}}_{i,j-\frac{1}{2}}\right)\left(Q^{n+\frac{1}{2}}_{i+\frac{1}{2},j} + Q^{n+\frac{1}{2}}_{i+\frac{1}{2},j-1}\right)\right]$$

$$+ \frac{\Delta t}{4\Delta S}\left[\left(\frac{\chi}{h+\eta}\right)^{n+1}_{i-\frac{1}{2},j-\frac{1}{2}}\left(P^{n+\frac{1}{2}}_{i,j-\frac{1}{2}} + P^{n+\frac{1}{2}}_{i-1,j-\frac{1}{2}}\right)\left(Q^{n+\frac{1}{2}}_{i-\frac{1}{2},j} + Q^{n+\frac{1}{2}}_{i-\frac{1}{2},j-1}\right)\right]$$

$$- \frac{\Delta t}{2\Delta S}\left[\left(\eta g\alpha^{y}_{1} + C^{2}\right)^{n+1}_{i-\frac{1}{2},j+\frac{1}{2}} + \left(\eta g\alpha^{y}_{1} + C^{2}\right)^{n+1}_{i-\frac{1}{2},j-\frac{1}{2}}\right]$$

$$\cdot\left[\left\{\eta^{n+1}_{i-\frac{1}{2},j+\frac{1}{2}} - \eta^{n+1}_{i-\frac{1}{2},j-\frac{1}{2}}\right\}\right] - \frac{\Delta t}{2\Delta S}\left[\left(\eta g\alpha^{y}_{2}\right)^{n+1}_{i-\frac{1}{2},j+\frac{1}{2}} + \left(\eta g\alpha^{y}_{2}\right)^{n+1}_{i-\frac{1}{2},j-\frac{1}{2}}\right]$$

$$\cdot\left[\left\{h^{n+1}_{i-\frac{1}{2},j+\frac{1}{2}} - h^{n+1}_{i-\frac{1}{2},j-\frac{1}{2}}\right\}\right] - \frac{1}{2}\varepsilon_{i-\frac{1}{2},j}Q^{n}_{i-\frac{1}{2},j} \qquad (34)$$

ΔS and Δt is the spatial and temporal increment, respectively and, n is the time step.

2.2 Initial and boundary conditions

As the initial conditions, the surface elevation η is given at $t = n\Delta t$ time step where the discharges at $t = (n + \frac{1}{2})\Delta t$ time level to initiate the computation.

Both incident and transmitted boundary conditions are introduced in terms of discharge per unit width. As the incident boundary condition of the x-direction we apply:

$$P_i = P_c + (C_i + C_r)\eta_i - C_r\eta \qquad (35)$$

where P_c is the current discharge, $\eta_i = a_i\cos(k_j x_j - \sigma t)$, a_i and C_i is the incident wave profile, its amplitude and celerity, respectively and C_r is the celerity of the reflected wave.

In the present application shown from section 3.2, an open boundary is assumed at the transmission region instead of an absorption boundary. An open boundary condition works well for the present case. For any different type of boundary condition, all the terms associated with the $\varepsilon(x)$ and $\varepsilon(y)$ in the momentum equations shall be eliminated. As the transmitted boundary condition we use:

$$P_t = P_c + C_t\eta_t \qquad (36)$$

where the subscript t stands for the component of the respective quantity at the transmitted boundary.

3. Application of the One Dimensional Wave-current Model

When we consider a one-dimensional phenomenon then the above mentioned equations turn into a new set of differential equations [Zaman et al. (1994) and Togashi et al. (1995)] where all terms related to y-direction including the y-direction momentum equation become obsolete. Subsequently, the continuity equation (Eq.14) and momentum equation (Eq.15) takes the following form:

$$\eta_t + P_x = 0 \tag{37}$$

$$P_t + \left[\frac{P^2 \chi}{h+\eta}\right]_x + [\eta g \alpha_1 + C]\eta_x + [\eta g \alpha_2]h_x + \varepsilon P = 0 \tag{38}$$

where the subscripts x and t stand for partial differentiation operator. χ is the momentum correction factor. α_1 and α_2 are the relative water depth dependent parameters and can be expressed as:

$$\chi = \frac{1}{2}\left[\frac{k(h+\eta)}{\tanh k(h+\eta)}\right]\left[1 + \frac{2k(h+\eta)}{\sinh 2k(h+\eta)}\right] \tag{39}$$

$$\alpha_1 = X - 1 \tag{40}$$

$$\alpha_2 = X - \frac{1}{\cosh k(h+\eta)} \tag{41}$$

and,

$$X = \left[\frac{2\tanh k(h+\eta) + \frac{2\sigma U}{g}\left(1 - \frac{kU}{\sigma}\right)}{k(h+\eta) + \frac{1}{2}\sinh 2k(h+\eta) + \frac{2\sigma U}{g}\left(1 - \frac{kU}{\sigma}\right)\cosh^2 k(h+\eta)}\right] \tag{42}$$

3.1 Numerical scheme

Discretization of Eqs.37 and 38 are performed following a semi-implicit finite difference technique. The computational mesh in the x-t plane is shown in Figure 2. The discharges P are defined at the integer grid points and fractional time steps (shown by ● in the mesh) and those of η are defined at the fractional grid points and integer time steps (shown by ■ in the mesh). After discretization Eqs.37 and 38 take the following forms:

$$\eta_{j+1/2}^{n+1} = \eta_{j+1/2}^n - \frac{\Delta t}{\Delta x}P_{j+1}^{n+1/2} + \frac{\Delta t}{\Delta x}P_j^{n+1/2} \tag{43}$$

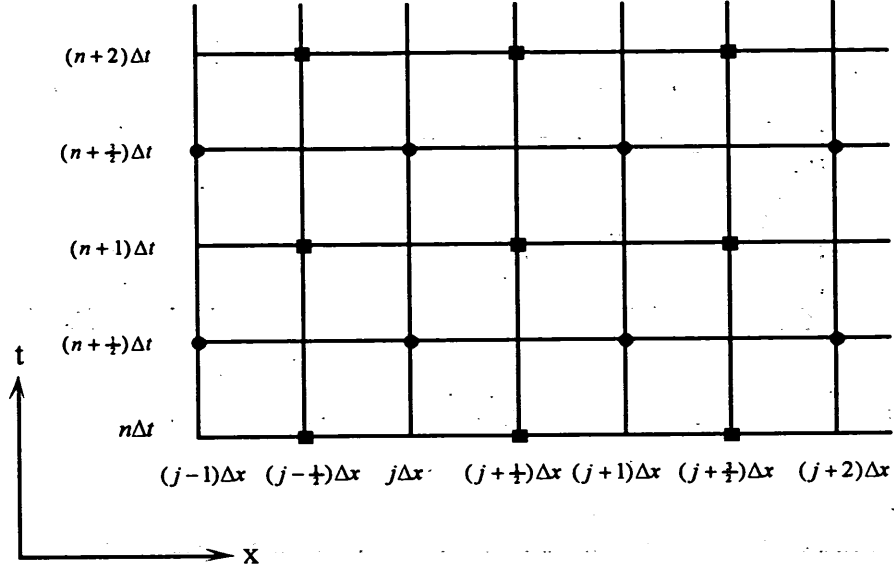$$A_j^{n+1}P_{j-1}^{n+3/2} + B_j^{n+1}P_j^{n+3/2} + C_j^{n+1}P_{j+1}^{n+3/2} = D_j^{n+1} \tag{44}$$

Figure 2 Definition sketch of the one-dimensional computational mesh

where,

$$A_j^{n+1} = -\frac{\Delta t}{4\Delta x}\left(\frac{\chi}{h+\eta}\right)_{J-1/2}^{n+1}\left(P_j^{n+1/2} + P_{J-1}^{n+1/2}\right)$$ (45)

$$C_j^{n+1} = \frac{\Delta t}{4\Delta x}\left(\frac{\chi}{h+\eta}\right)_{J-1/2}^{n+1}\left(P_{J+1}^{n+1/2} + P_j^{n+1/2}\right)$$ (46)

$$B_j^{n+1} = 1 + A_j^{n+1} + C_j^{n+1} + \frac{1}{2}\varepsilon_j$$ (47)

$$D_j^{n+1} = P_j^{n+1/2} - \frac{\Delta t}{2\Delta x}\left[\left(C^2 + \chi_1 g\eta\right)_{J+1/2}^{n+1} + \left(C^2 + \chi_1 g\eta\right)_{J-1/2}^{n+1}\right]\left(\eta_{J+1/2}^{n+1} - \eta_{J-1/2}^{n+1}\right)$$

$$- \frac{\Delta t}{2\Delta x}\left[\left(\chi_2 g\eta\right)_{J+1/2}^{n+1} + \left(\chi_2 g\eta\right)_{J-1/2}^{n+1}\right]\left(h_{J+1/2} - h_{J-1/2}\right) - \frac{1}{2}\varepsilon_j P_j^{n+\frac{1}{2}}$$ (48)

The computational tactics of this model is, η, at time level $(n+1)\Delta t$ will be evaluated by the Eq.43 with the known value of η at $n\Delta t$ time level and, P at $(n+\frac{1}{2})\Delta t$ time level and then, Eq.44 is employed to estimate P for $(n+\frac{3}{2})\Delta t$ time level, using the calculated η at $(n+1)\Delta t$ time level. The coupling of the above equations will continue until a steady state is reached.

3.2 Application of the model

As an application of the model established in the previous section we choose a case where waves ride over a steady current and subsequently they interact with each other in the presence of a submerged bottom seated obstacle. The computational domain is described in Figure 3, where l is the obstacle length, h the still water depth over the flat bottom, rh the obstacle height, r is the ratio of the obstacle height to the water depth and U is the uniform current.

e

e

e

e

e

e

e

e

e

e

e

e

e

e

e

e

e

e

e

e

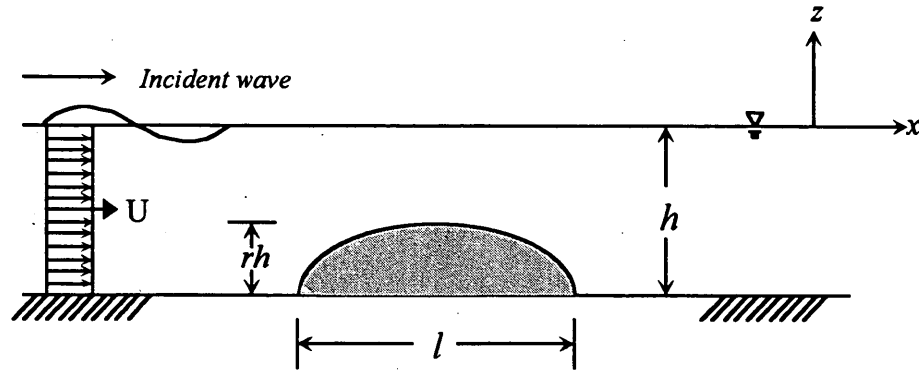.

Figure 3 Schematic view of the computational domain

3.3 Experimental setup

We use 15 capacitance type wave gauges to measure the surface elevations at fifteen different positions in the wave channel over and, both upstream and downstream sides of the obstacle. Setup of the wave gauges is shown in **Figure 4** where it could be seen that five wave gauges are set in the upstream side of the obstacle, 5 over the obstacle and the rest 5 are put in the downstream part. The spacing between the successive wave gauges is 30cm.
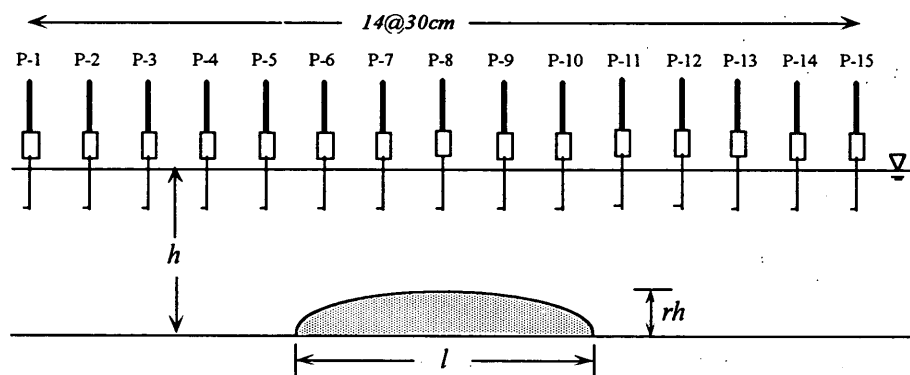
Figure 4 Setup of the wave gauges

3.4 Computational conditions

In terms of non-dimensional parameters, U/C_i alters to 0.14, 0.18 and 0.22 while the relative water depth h/L_i is 0.3, the wave steepness H_i/L_i is 0.03, the relative obstacle height r is 0.5 and the relative obstacle length rh/l is 0.2. Here L_i and H_i are the length and height of the incident waves in the absence of current. In order to verify the applicability of the above described numerical model, relevant experiments [Zaman and Togashi (1996)] are performed in a large scale computer controlled wave channel.

3.5 Treatment to flow separation

Due to the flow separation, it is observed by means of the injected dye that the reverse flow close to the bottom is quite significant over the lee side and close vicinity of the obstacle. It decreases slowly and diminishes at some distance from the obstacle over the flat bottom. The intensity and the extent of this reverse flow are found to be well related with the magnitude of the current. Due to the reverse flow the main forward flow feels the bottom not at the physical bottom but a little above and along the layer between the forward and reverse flow. This situation virtually

reduces the water depth from the bottom in these region results to an increase of the mean velocity of the main forward flow to maintain the continuity. The physical problem is shown in **Figure 5**. We have tried to find a solution of this problem geometrically through locating the two ends of the reverse flow zone starts from the obstacle body to the flat bottom. We have started with our experimental data and establish two equations (Eqs.49 and 50) which will account the effect of flow separation on the current velocity and consequently on the wave height and mean water level.

Wave direction
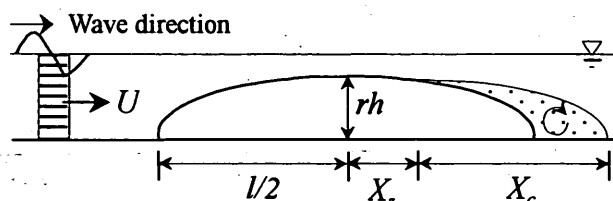
Figure 5 Flow separation.

$$X_c = 18rh\left[1 - \frac{24.15}{U}\right] \; ; \quad U > 24.15cm/s \qquad (49)$$

$$X_z = \frac{l}{2} - X_c\frac{rh}{l} \qquad (50)$$

where X_z is the distance from the top of the obstacle where separation starts and X_c is its length. We use three different types of current velocity (U=24.15cm/s, 31.05cm/s and 37.79cm/s) in the experiment to perceive the phenomenon. We could not go beyond this current limit. This is because the wave channel where the experiments are performed, the vertical distribution of the current velocity loses its uniformity when the current velocity exceeds 40cm/s. Again when the current velocity is about 24.15cm/s (Reynold number is 0.7245×10^6), reverse flow is found to take place insignificantly. So we use the current velocity 24.15cm/s as the base line of our new equations. Eqs. 49 and 50 are obtained from the experimental data those we currently have. Use of extensive data both for varying currents and bottom topographies may reproduce generalized version of the above two equations. In this research Eqs.49 and 50 are found very useful to minimize the discrepancies in the wave heights and mean water levels due to flow separation in the downstream side of the obstacle.

3.6 Results and analyses
3.6.1 Linearized model

Initially we linearize our momentum equation (Eq.38) and compute the wave components for $U/C_i = 0.14$ and 0.22 while $h/L_i = 0.3$, $H_i/L_i = 0.03$, $r = 0.5$ and $rh/l = 0.2$ as the test cases to perceive the applicability of linearized model. **Figures 6** compare the nonlinear model, linearized model and experimental results. **Figures 6a** and **6b** compare the normalized surface elevations at the top of the obstacle, respectively. **Figures 6c** and **6d** respectively describes the discrepancies of the wave heights of the above cases. **Figures 6e** and **6f** respectively show the comparisons of the mean water levels.
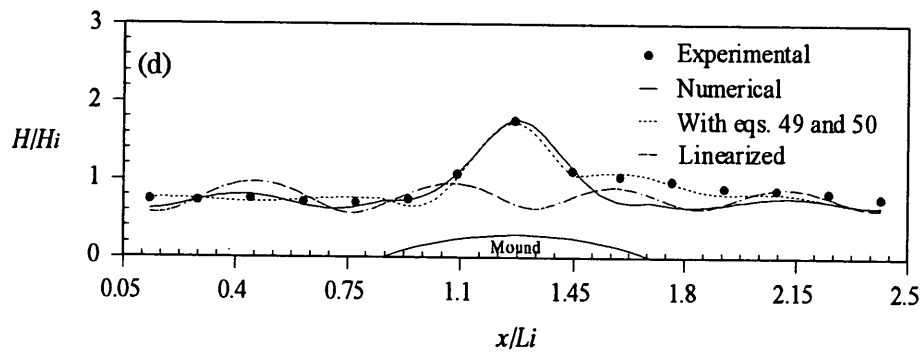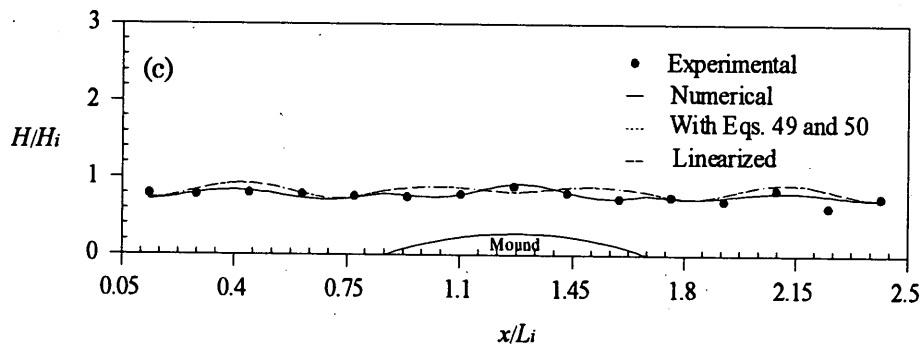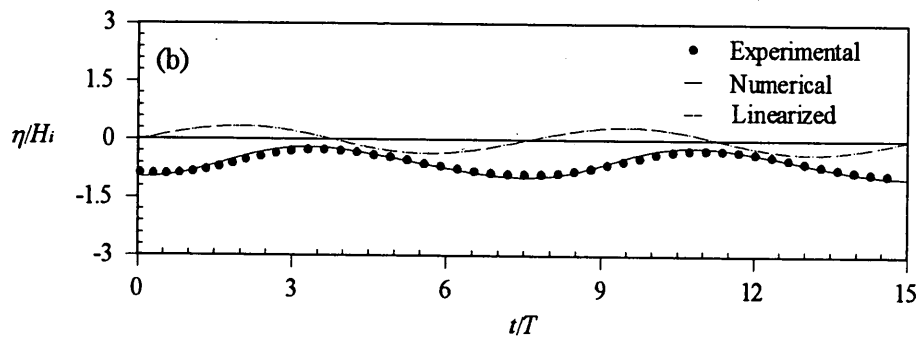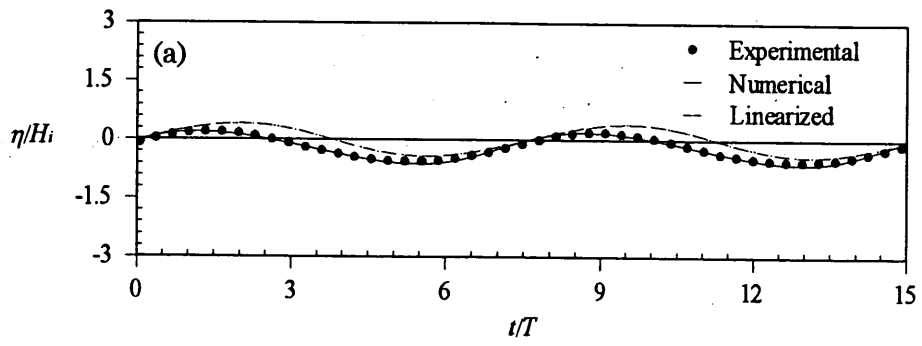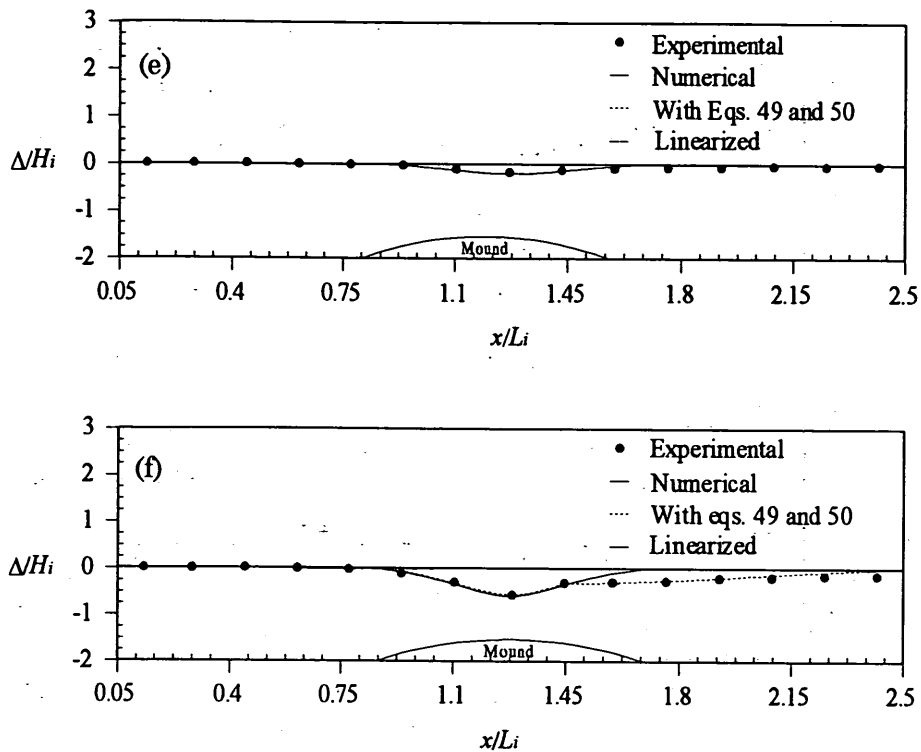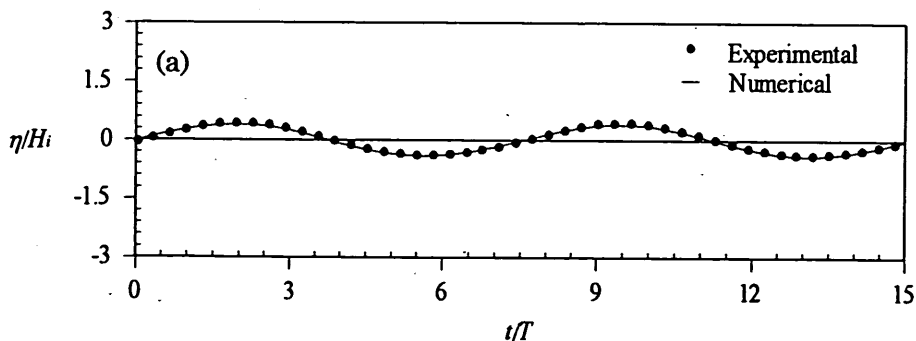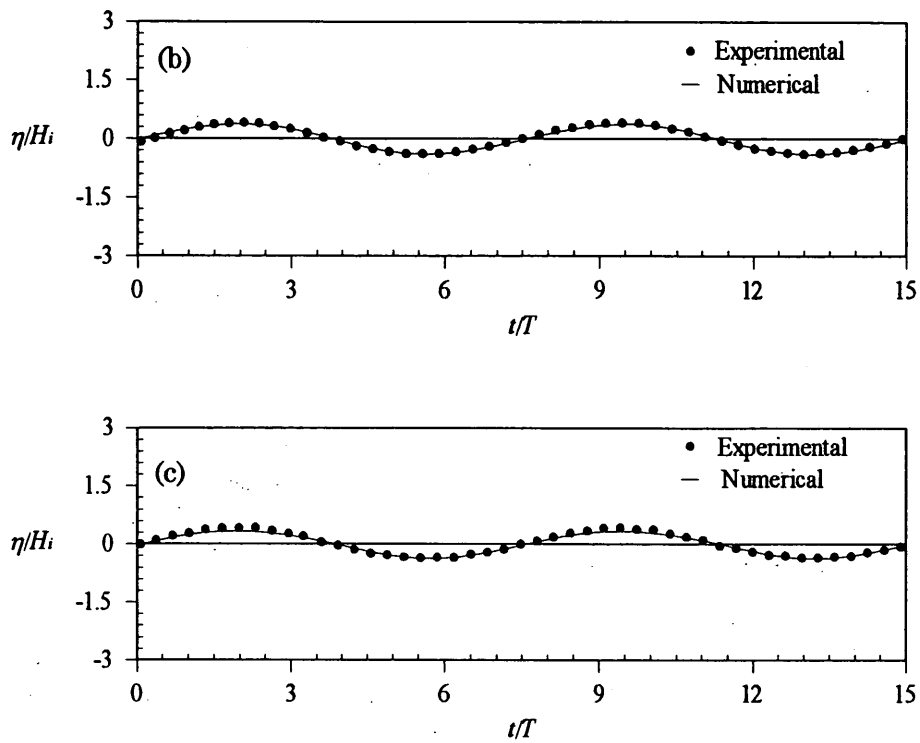
Figure 6: (a) Comparison of surface elevations at top of the obstacle $(U/C_i = 0.14)$; (b) Comparison of surface elevations at top of the obstacle $(U/C_i = 0.22)$; (c) Comparison of wave heights $(U/C_i = 0.14)$; (d) Comparison of wave heights $(U/C_i = 0.22)$; (e) Comparison of mean water levels $(U/C_i = 0.14)$, and (f) Comparison of mean water levels $(U/C_i = 0.22)$

It may be noted from the figures that linearized model can fairly predict the wave evolution during passage over a submerged parabolic obstacle when the current velocity is not strong enough. But it is not effective in the presence of large current velocity resulting to a mismatch of the surface elevations and other wave characteristics. In the case of linearized model, the drop of the mean water levels doesn't also appear in spite of the magnitude of the current velocity due to the absence of higher order terms.
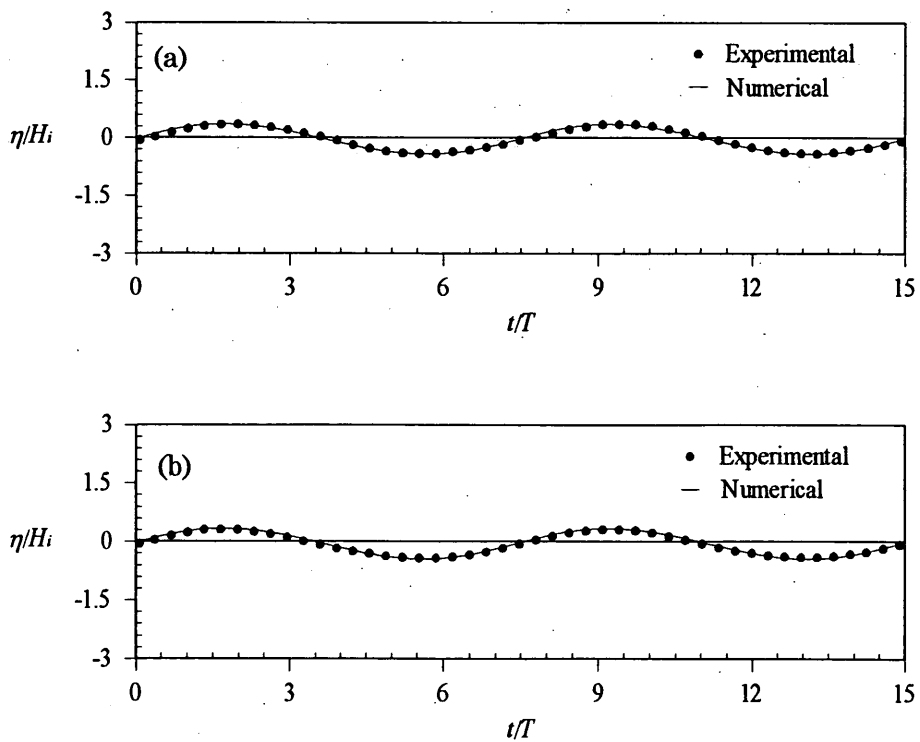
3.6.2 Comparisons of surface elevations using nonlinear model

The numerical and experimental results for varying forced currents (U/C_i) are compared at seven different points in the wave channel. These positions are defined as, at the entrance of the domain (P-1) and over all points of the obstacle (P-6, P-7, P-8, P-9 and P-10).

Figure 7 Comparison of surface elevation at point P-1:
(a) $U/C_i = 0.14$, (b) $U/C_i = 0.18$ and (c) $U/C_i = 0.22$;
($h/L_i = 0.3, H_i/L_i = 0.03, r = 0.5$ and $rh/l = 0.2$)

In the comparisons of the surface elevations, it is observed that on the flat bottom and up to the top of the

obstacle the prescribed nonlinear model is enough to predict the wave evolution but fails when the flow separation is stronger in the down downstream side. The discrepancies in the results can be almost overcome when Eqs. 49 and 50 are invoked in the original model (*see* Figures 12b and 12c).
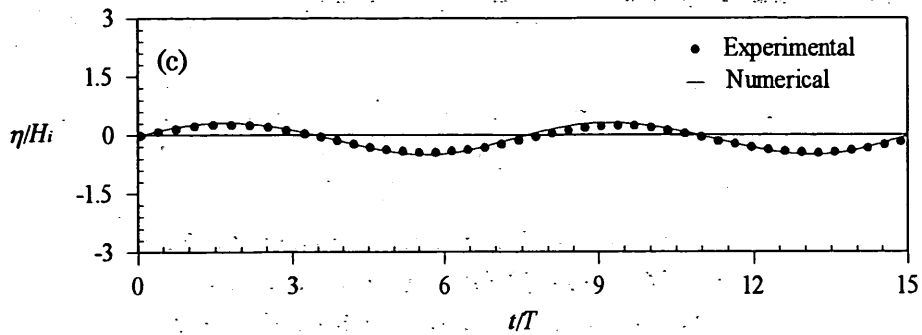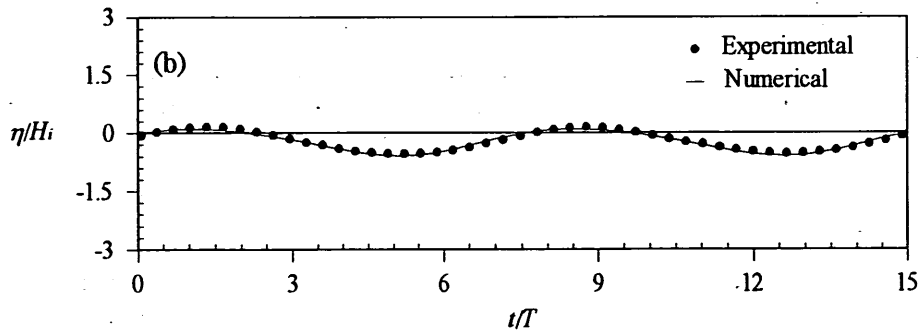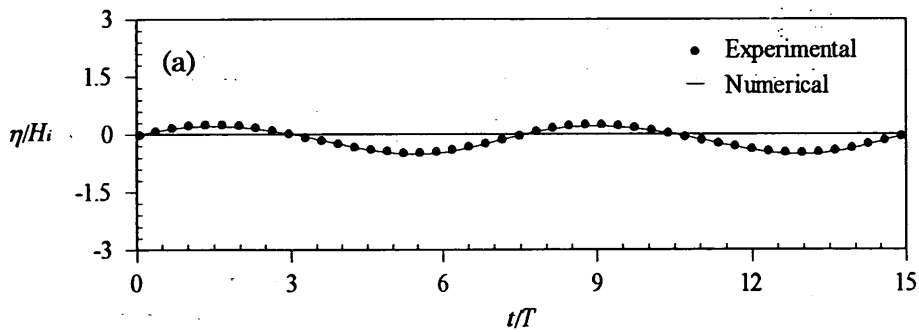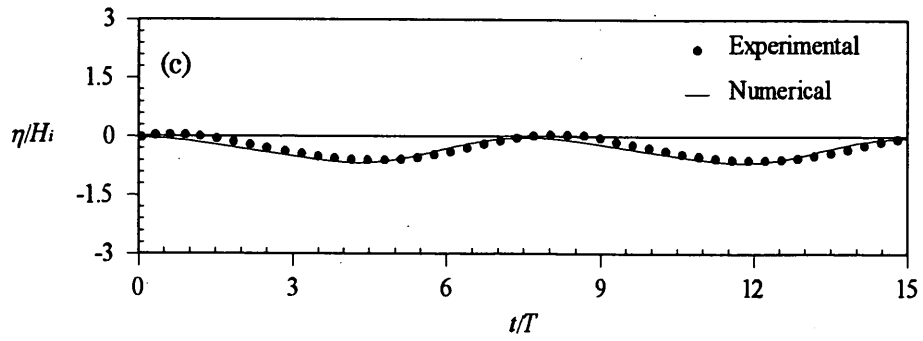
Figure 8 Comparison of surface elevation at point P-6:
(a) $U/C_i = 0.14$, (b) $U/C_i = 0.18$ and (c) $U/C_i = 0.22$;
(h/L_i = 0.3, $H_i/L_i = 0.03$, $r = 0.5$ and $rh/l = 0.2$)

Figure 9 Comparison of surface elevation at point P-7:
(a) $U/C_i = 0.14$, (b) $U/C_i = 0.18$ and (c) $U/C_i = 0.22$;
($h/L_i = 0.3, H_i/L_i = 0.03, r = 0.5$ and $rh/l = 0.2$)

Figure 10 Comparison of surface elevation at point P-8:
(a) $U/C_i = 0.14$, (b) $U/C_i = 0.18$ and (c) $U/C_i = 0.22$;
($h/L_i = 0.3, H_i/L_i = 0.03, r = 0.5$ and $rh/l = 0.2$)

Figure 11 Comparison of surface elevation at point P-9:
((a) $U/C_i = 0.14$, (b) $U/C_i = 0.18$ and (c) $U/C_i = 0.22$;
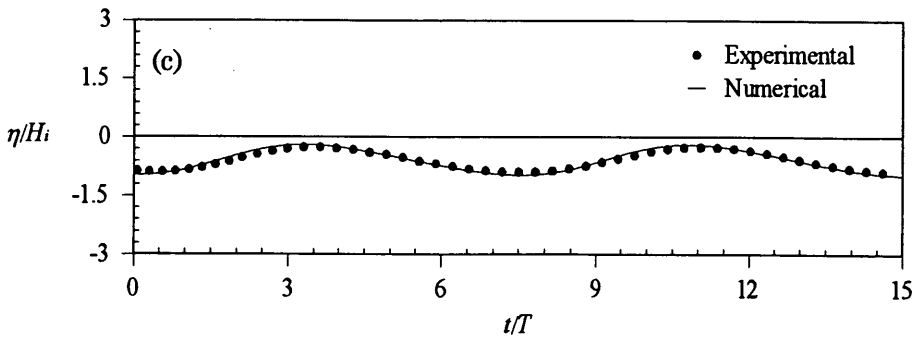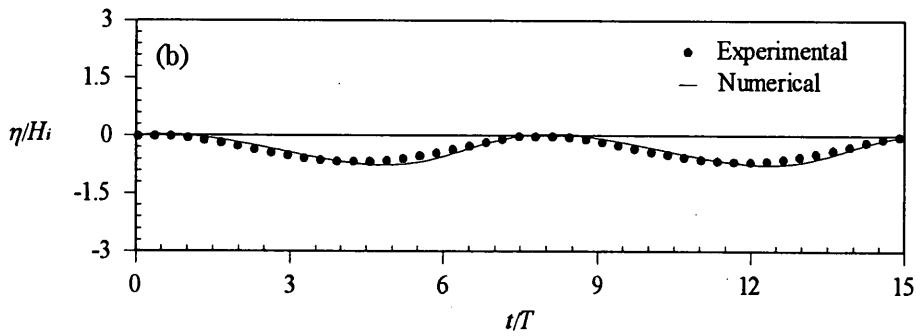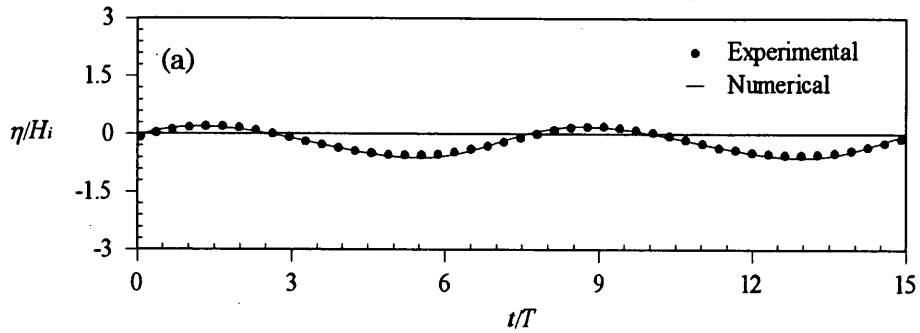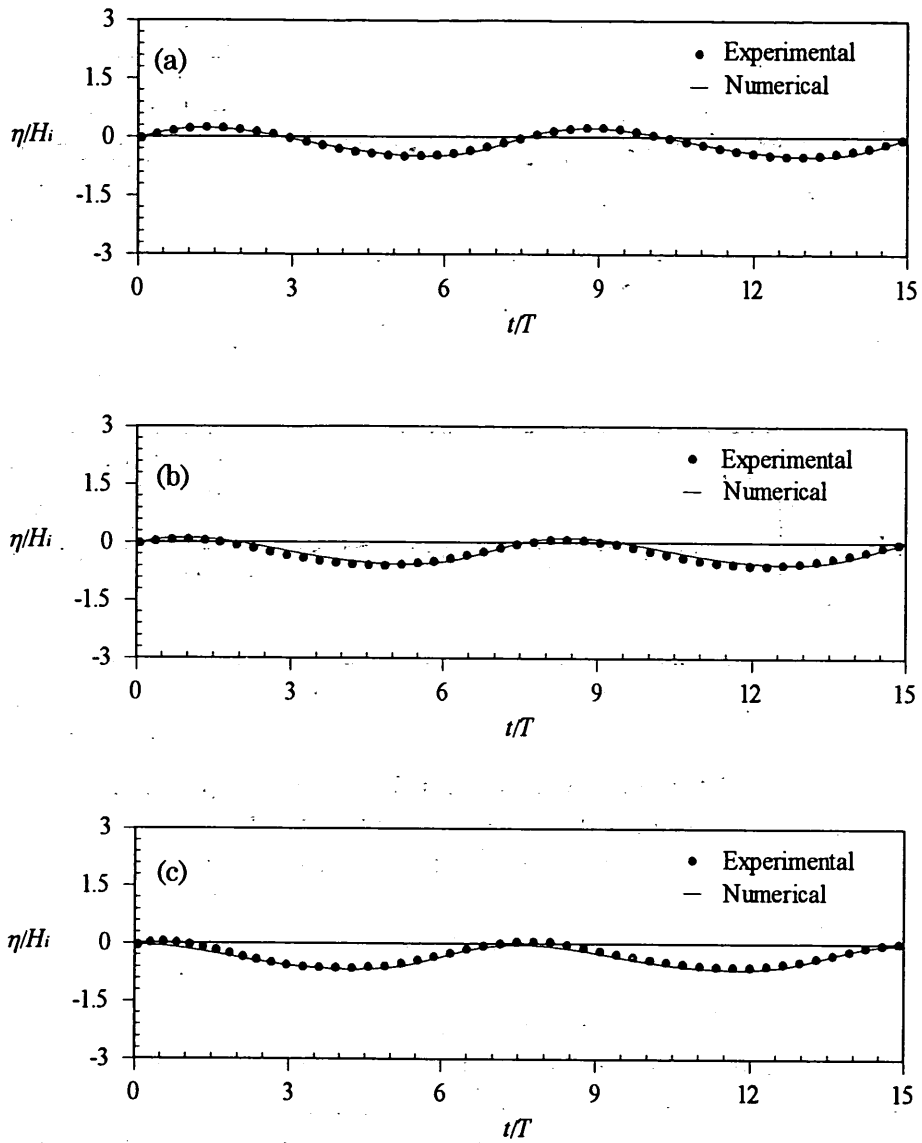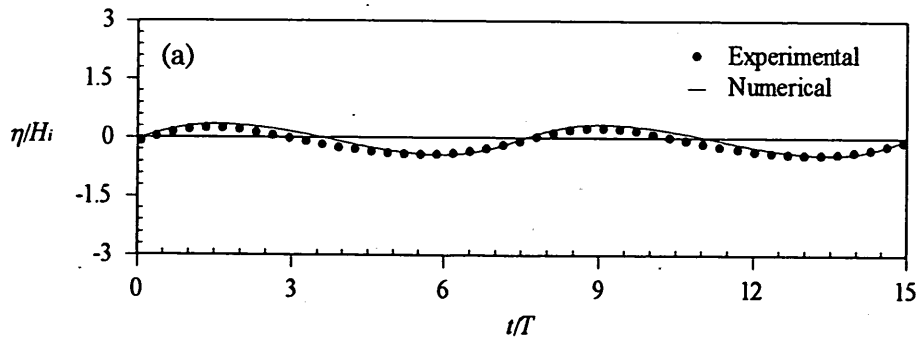($h/L_i = 0.3$, $H_i/L_i = 0.03$, $r = 0.5$ and $rh/l = 0.2$)
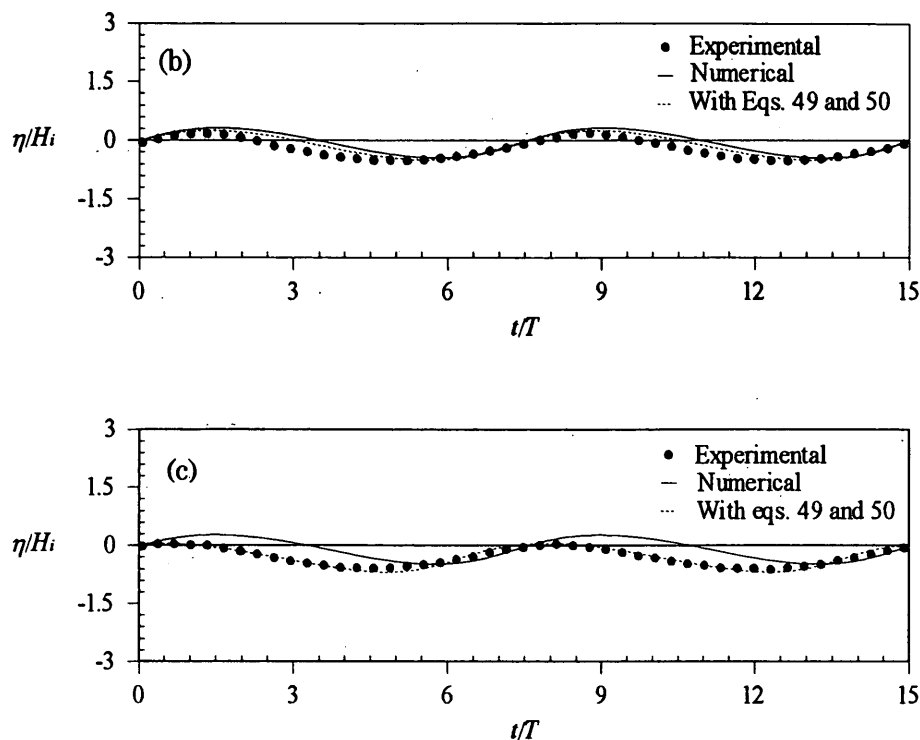
Figure 12 Comparison of surface elevation at point P-10:

(a) $U/C_i = 0.14$, (b) $U/C_i = 0.18$ and (c) $U/C_i = 0.22$;

$(h/L_i = 0.3, H_i/L_i = 0.03, r = 0.5$ and $rh/l = 0.2)$

4. Conclusion

The governing equations of this mathematical model are obtained through the vertical integration of the continuity equation and the equation of motion. A semi-implicit finite difference method has been proposed for the numerical solution of the resulted equations. As an application, the established model is utilized to study the strongly interacted waves and currents over a submerged obstacle of parabolic cross section. Relevant experiments are also performed to account the applicability of the proposed model. Flow separation phenomenon is considered geometrically with two equations obtain from the experimental data. The numerical results are shown to be in great agreement with the experiments. Linearized form of the model is found to be ineffective in reproducing the wave evolution during passage over the obstacle in the presence of stronger current.

Acknowledgements

References

Brevik, I. and B. Aas (1980), "Flume experiment on waves and currents. I. rippled bed," *Coast. Eng., Elsevier Sci. Pub. Co.,* Vol. 3, pp.149-177.

Brevik, I. (1976), "The stopping of linear gravity waves in currents of uniform vorticity," *Physica Norvigica,* Vol.8(3), pp.157-162.

Dean, R. G. & R. A. Dalrymple (1992), "Water wave mechanics for engineers and scientists," *JBW Printers and Binders,* pp.66-69.

Hedges, T. S. (1987), "Combination of waves and currents: an introduction," *Proc. Int. Civ. Engrs, Part 1,* Vol.82, pp.567-585.

Hedges, T. S. and B. W. Lee (1991), "The equivalent uniform in wave-current computations," *Coast. Eng., Elsevier Sci. Pub. B. V.,* Vol.16, pp.301-311.

Horikawa, K. (1988), "Nearshore dynamics and coastal processes," University of Tokyo press, pp.522.

Ismail, N. M. (1983), "Effects of wave-current interaction on the design of marine structure,"*Offshore Tech. Conf.,* pp.307-313.

Longuet-Higgins, M. S. and R. W. Stewart (1961): "The changes in amplitude of short gravity waves on steady non-uniform currents," *J. Fluid Mech.,* Vol.10, pp.529-549.

Longuet-Higgins, M. S. and R. W. Stewart (1962), "Radiation stress and mass transport in gravity waves with application to surf beats," *J. Fluid Mech.,* Vol.13, pp.481.

Longuet-Higgins, M. S. and R. W. Stewart (1963), "A note on wave set-up," *J. Marine Res.,* Vol.21, pp.9.

Longuet-Higgins, M. S. and R. W. Stewart (1964), "Radiation stress in water waves, a physical discussion with application," *Deep-Sea Res.,* Vol.11, pp.529.

Madsen, P. A. and O. R. Sørensen (1992), "A new form of the Boussinesq equations with improved linear dispersion characteristics. Part 2. A slowly varying bathymetry," *Coast. Eng., Elsevier Sci. Pub,* 18, pp.183-204.

McCowan, A. D. (1987), "The range of application of Boussinesq type numerical short wave models," *Proc. 22nd IAHR Congr., Laussane,* pp.378-384.

Ribberink, J. S., I. Katopodi, K. A. H. Ramadan, R. Koelewijn and S. Longo (1994), "Sediment transport under (non)-linear waves and currents," *Proc. 24th Coast. Eng. Conf.,* pp.2527-2541.

Sato, S and M. B. Kabiling (1994), "A numerical simulation of beach evolution based on a nonlinear dispersive wave-current model," *Proc. 24th Conf. Coast. Eng.,* Kobe, pp.2557-2570.

Schäffer, H. A. and P. A. Madsen (1995), "Further enhancements of Boussinesq-type equations," *Coast. Eng., Elsevier Sci. B. V.*, 26, pp.1-14.

Sørensen, O. R., H. A. Schaffer, P. A. Madsen and R. Deigaard (1994), "Wave breaking and induced nearshore circulations," *Proc. 24th Conf. Coast. Eng.*, Kobe, pp.2583-2594.

Skop, R. A. (1987), "Approximate dispersion relation for wave current interaction, *"J. Wtrwy., Port, Coast., and Oc, Engng*, Vol.113, No.2, pp.187-195.

Togashi, H., M. H. Zaman and X. Yu (1995), "Wave-current interaction over a submerged mound of trapezoidal cross section," Advances in Hydro-Science and-Engineering, Vol.II, Part B, *Proc. 2nd Int. Conf. on Hydro-Sci. and -Eng.*, CHES and IRTCES (ed.), Beijing, China, pp.1452-1459.

Watanabe, A., K. Shiba and M. Isobe (1994), "A numerical model of beach change due to sheet-flow," *Proc. 24th Coast. Eng. Conf.*, pp.2785-2798.

Yoon, S. B. and P. L.-F. Liu (1989), "Interactions of currents and weakly nonlinear water waves in shallow water," *J. Fluid Mech.*, 205, pp.397-419.

Zaman, M. H., H. Togashi and X. Yu (1994), "Modeling wave current interaction over an uneven sea bottom," *Proc. Civil. Eng. in the Ocean, JSCE*, Vol.10, pp.25-30.

Zaman, M. H. and H. Togashi (1996), "Experimental study on interaction among waves, currents and bottom topography," *Proc. Civil. Eng. in the Ocean, JSCE*, Vol.12, pp.49-54.

Zaman, M. H. and H. Togashi (1997), "Modeling horizontally two dimensional wave-current coexistence field over uneven topography," *Proc. 7th Int. Offshore and Polar Eng. Conf.*, ISOPE-97, Vol.III, pp.838-845

List of symbols

The following symbols are used in the present paper:

A	:	arbitrary constant related to wave height
A_j	:	constant
a_i	:	amplitude of the incident wave
B_j	:	constant
C	:	wave celerity
C_i	:	celerity of the incident wave
C_j	:	constant
C_r	:	celerity of the reflected wave
C_t	:	celerity of the transmitted wave
D_j	:	constant
g	:	acceleration due to gravity
H_i	:	incident wave height
h	:	still water depth

j	:	horizontal x-grid point
k	:	wave number
L_i	:	incident wavelength
χ	:	momentum correction factor
n	:	computational time step
p_d	:	dynamic pressure
P	:	flux in the x-direction
P_i, P_t	:	fluxes at the x-incident and x-transmitted boundary
P_c	:	current discharge
Q	:	flux in the y-direction
r	:	ratio of obstacle height to still water depth
R	:	a coefficient
rh	:	maximum height of the obstacle
ΔS	:	space increment
t	:	time
T	:	wave period
Δt	:	time increment
u	:	velocity component in the x direction
u^b	:	magnitude of u at bottom
u^s	:	magnitude of u at surface
v^b	:	magnitude of v at bottom
v^s	:	magnitude of v at surface
U_x	:	velocity of the current in the x-direction
V_y	:	velocity of the current in the y-direction
w	:	velocity component in the z direction
w^b	:	magnitude of w at bottom
w^s	:	magnitude of w at surface
x	:	horizontal axis
X	:	constant
Δx	:	horizontal space increment
Y	:	constant
z	:	vertical axis
ϕ	:	velocity potential for wave-current field
η	:	surface fluctuation
η_i	:	surface fluctuation due to incident wave
η_t	:	surface fluctuation due to transmitted wave
α^x_1	:	relative water depth dependent parameter for x-direction
α^x_2	:	relative water depth dependent parameter for x-direction
α^y_1	:	relative water depth dependent parameter for y-direction
α^y_2	:	relative water depth dependent parameter for y-direction
ρ	:	water density
σ	:	angular frequency
$\varepsilon(x)$	:	boundary-damping function
$\varepsilon(y)$	:	boundary-damping function
ε_m	:	damping coefficient